Structure of the Cdc48 segregase in the act of unfolding an authentic substrate

Ian Cooney[1,*], **Han Han**[1,*], **Michael G. Stewart**[1], **Richard H. Carson**[2], **Daniel T. Hansen**[1], **Janet H. Iwasa**[1], **John C. Price**[2], **Christopher P. Hill**[1,†], **Peter S. Shen**[1,†]

[1]Department of Biochemistry, 15 N. Medical Drive East, University of Utah, Salt Lake City, UT 84112, USA.

[2]Department of Chemistry and Biochemistry, C100 BNSN, Brigham Young University, Provo, UT 84602, USA.

Abstract

The cellular machine Cdc48 functions in multiple biological pathways by segregating its protein substrates from a variety of stable environments such as organelles or multi-subunit complexes. Despite extensive studies, the mechanism of Cdc48 has remained obscure, and its reported structures are inconsistent with models of substrate translocation proposed for other AAA+ ATPases (adenosine triphosphatases). Here, we report a 3.7-angstrom–resolution structure of Cdc48 in complex with an adaptor protein and a native substrate. Cdc48 engages substrate by adopting a helical configuration of substrate-binding residues that extends through the central pore of both of the ATPase rings. These findings indicate a unified hand-over-hand mechanism of protein translocation by Cdc48 and other AAA+ ATPases.

Cdc48 (human homolog known as p97/VCP) is an abundant and essential AAA+ ATPase (adenosine triphosphatase) that separates protein substrates from complexes, organ-elle membranes, chromatin, and ribosomes (1). This activity is important in a wide range of cellular processes that can be dependent or independent of ubiquitylation, including protein quality control, regulated proteolysis, and ribo-some quality control, with recruitment of Cdc48 to its different functions being mediated by a variety of adaptor proteins (2). Cdc48/p97 mutations are linked to multiple diseases (3), including multisystem proteinopathy, familial amyotrophic lateral sclerosis, and Charcot-Marie-Tooth disease type 2Y, and Cdc48/p97 is an established target for the development of cancer therapeutics (4).

Cdc48 comprises an N-terminal (N) domain followed by two ATPase cassettes (D1 and D2) (Fig. 1A). In marked contrast to published structures of Cdc48/p97 hexamers, which all display sixfold rotational symmetry (5–10), several other AAA+ structures display an asymmetric architecture that suggests a hand-over-hand mechanism of substrate translocation (11). Prompted by this discrepancy, we reasoned that the absence of bound substrate might have allowed the currently available Cdc48 structures to adopt an inactive conformation. We therefore rapidly purified Cdc48 complexes from *Saccharomyces cerevisiae* by co-immunoprecipitation (co-IP) of the substrate-recruiting adaptor Shp1 (12) (fig. S1) and determined the structure by electron cryo-microscopy (cryo-EM). Co-IPs were per formed in the presence of the nucleotide analog ADP•BeF$_x$, which supports substrate binding to the related ATPase Vps4 (13).

Two distinct structures were determined at resolutions of 3.7 and 4.5 Å (figs. S2 to S4 and supplementary materials and methods). The 4.5-Å structure lacks density for substrate, is rotationally symmetric, and superimposes with previously reported structures. By contrast, the 3.7-Å structure displays an asymmetric configuration and density for polypeptide substrate that passes through the pores of both the D1 and D2 rings (Fig. 1B and movies S1 to S3). It therefore represents an active, substrate-processing conformation, whereas the symmetric reconstruction, which will not be discussed further, represents a state that is not engaged with substrate.

The D1 and D2 rings are crowned by the N domains, the density of which is relatively weak but appears to show bound Shp1 UBX domain for at least some of the subunits, and is especially clear for subunit B (Fig. 1 and fig. S5). This positioning of the N domains in the "up" conformation is consistent with our structure being in a substrate-engaged conformation and the finding that disease-related mutations deregulate human Cdc48/p97 by disrupting partitioning to the repressed "down" conformation (14). Segments of substrate outside of the Cdc48 pore and the other domains of Shp1 are presumably mobile, which is consistent with a cloud of low threshold density above the mouth of the D1 ring (Fig. 1C).

The D1 and D2 domains of five of the six subunits (A to E) adopt a helical symmetry, whereas the sixth subunit (F) occupies two positions (F$_1$ and F$_2$) that are displaced from the substrate and the helix axis (Figs. 1 and 2 and figs. S6 and S7). D1 and D2 display a relative rotation of just ~20° when viewed along the helical axis. Interfaces between subunits A to E are stabilized by ADP•BeF$_x$, whose coordination at the ATPase sites of subunits A to D is completed by the finger arginine residues from the following subunit (Fig. 2B and fig. S8).

Thus, ADP•BeF$_x$ supports close packing between adjacent large ATPase domains for subunits A to E (Fig. 2C). By contrast, subunit F contacts its neighboring E and A subunits primarily through interactions involving the small ATPase domains toward the periphery of the rings and displays gaps between large domains of adjacent subunits (Fig. 2D). At the subunit E ATPase site, density is clear for just two phosphates, and the nucleotide is modeled as ADP in both D1 and D2 (fig. S8). At subunit F, poor density does not permit building a reliable model for nucleotide.

Connections between D1 and D2 are superimposable for subunits A to D. Following D1, residues 470 to 484 form a linker comprising two turns and an extended section (Fig. 2E). Near the start of the linker, L474 packs against a hydrophobic surface on its own D2 and R475 packs against D1 of the following subunit. The extended section packs three hydrophobic side chains (V479, V482, and V484) against its D2 cassette and residues centered on M621 from D2 of the following subunit. These contacts, along with a small (~200 Å^2) interface centered on residues 318 and 414 to 415 of D1 and 546 to 548 and 578 to 579 of D2, define the relative orientation of D1 and D2 for subunits A to E (Fig. 2E). By contrast, the subunit E linker mostly lacks density, which indicates increased flexibility due to the loss of contacts with the following F subunit. Thus, the linker defines the relative orientation of D1 and D2 rings by packing against D1 and D2 of their own subunit and at the interface between neighboring subunits.

Pore loop 1 residues of successive A to E subunits are related by 60° rotation and 6.8-Å translation in a helical pattern that continues through D1 and D2, with breaks at subunit F (Fig. 3). This symmetry allows substrate to bind in a b-strand conformation, with each subunit contributing to binding of successive dipeptides (15, 16); accordingly, 22 residues of substrate were built in this conformation through the pore (Fig. 3A). The fit to density was generally good (fig. S9), especially for residues 11 to 22 in the D2 ring, although density was lacking for residues 9 and 10 at the junction between D1 and D2. The b-strand conformation is mechanistically appealing because it is a low-energy state for all amino acid residues, with some distortion required for proline, and is therefore suitable for binding and translocating a wide range of sequences.

Substrate density does not indicate specific residue types, probably at least in part because of a mixture of sequences and their registers.Another ambiguity is the substrate orientation, which we have modeled N to C (D1 to D2), but this remains an important question for future studies.

Substrate side chains bind between pore loop 1 residues of adjacent subunits, with successive substrate dipeptides binding at successive subunit interfaces. The first residue of each substrate dipeptide binds to a class 1 site, which is formed primarily by M288 (D1) and W561 (D2), whereas the second residue binds to a class 2 site, which is formed primarily by A289 (D1) and Y562 (D2) (16) (Fig. 3, B and C). Class 1 sites are flanked by K287 (D1) and M560 (D2). Class 2 sites are flanked by residues of pore loop 2, although in general their density is not well defined. Thus, the helical stack of subunits A to E presents an array of class 1 and class 2 pockets that can bind essentially any type of amino acid, with polar groups accommodated by hydrogen-bonding water molecules from the highly solvated pore.

Human Cdc48/p97 functions with the Shp1 homologs p37, p47, and UBXN2A to dissociate the I3 maturation factor from the inactive protein phosphatase 1 (PP1)-SDS22-I3 complex (17). Consistent with this, co-IP of Shp1-FLAG in the presence of ADP•BeF$_x$ resulted in enrichment of the homologous yeast complex: Glc7/PP1-Sds22-Ypi1/I3 and the related phosphatases Ppz1, Ppz2, and Ppq1 (fig. S10). By contrast, co-IP in the absence of ADP•BeF$_x$ did not enrich PP1 components and resulted in a C6-symmetric, substrate-free state of Cdc48 (figs. S10, C and D, S11). These observations reinforce the conclusion that the Shp1-Cdc48 complex described here represents an active conformation engaged with an authentic substrate, although definitive identification of the substrate engaged with the Cdc48 translocation pore is beyond the resolution of the current reconstruction. The enrichment of additional Cdc48 adaptors in the Shp1 co-IP is consistent with a hierarchical mode of cofactor binding (18), and the enrichment of multiple PP1 complex components is consistent with the reconstructed complex representing states in which the substrate is not yet completely processed.

The structure implies a hand-over-hand mechanism of translocation (Fig. 4 and movies S4 and S5). The snapshot captured in the structure shows subunits A to E gripping the substrate while the two conformations of subunit F are disengaged from substrate and lie on the path from binding the substrate dipeptide immediately after subunit E toward binding the dipeptide immediately before subunit A (Fig. 4A). In this model, the AB, BC, CD, and DE interfaces are stabilized by binding ATP at the A, B, C, and D active sites, respectively. Hydrolysis at the D active site weakens the DE interface to allow subunit E to move to the transitioning F state. This opens the interface to exchange ADP with ATP and subsequently dock against subunit A. The structure indicates a high degree of coordination between the D1 and D2 rings, although the extent to which their activity is coordinated remains to be determined.

The model holds that directionality of translocation results from hydrolysis occurring at the D-subunit active site or at a point shortly thereafter along the reaction path. The basis for hydrolysis specifically at this site is speculative because the A, B, C, and D active sites are superimposable at the current resolution. Consistent with a recent study on Vps4 (19), one possibility is indicated by the observation that the subunit E small domain undergoes a relative movement that is coupled to progression of subunit F, which suggests that progression along the transitioning pathway might be coupled to the conformational change of catalysis at the subunit D ATPase site (fig. S12).

Biochemical studies indicate that the D2 ring is more important for substrate translocation than is the D1 ring (20, 21). This is consistent with the less strong substrate density in D1 (Fig.1B and movie S3) and the identity of pore loop 1 residues, which in D2 are aromatic (W561 and Y562) and seem optimal for substrate binding. By comparison, in D1, these residues are flexible or small (M288 and A289), presumably bind substrate less tightly, and are more prone to slippage (22). This may facilitate the release of proteins from D1 that do not display an easily unfolded segment that can extend to the D2 pore loops.

Our approach of rapidly purifying a substrate adaptor in the presence of ADP•BeF$_x$ captured an active Cdc48 conformation in the act of translocating an authentic substrate. The structure

resembles other AAA+ ATPases that have been reported recently in the presence of substrate, including Vps4 (15, 16), YME1 (23), proteasome (24, 25), VAT (26), Hsp104 (27), ClpB (28, 29), and NSF (30) (fig. S13). This indicates that Cdc48/p97 uses the same hand-over-hand mechanism as these other AAA+ ATPases (11). Future priorities include determining the mechanism of substrate engagement and translocation in the presence of other adaptor/activators, resolving how pathogenic missense mutations in human p97 affects its substrate-processing functions, and leveraging the new structural insights in the development of Cdc48/p97 inhibitors that have potential as therapeutic agents (4).

Supplementary Material

Refer to Web version on PubMed Central for supplementary material.

ACKNOWLEDGMENTS

REFERENCES AND NOTES

1. Ye Y, Tang WK, Zhang T, Xia D, Front. Mol. Biosci 4, 39 (2017). [PubMed: 28660197]

2. Buchberger A, Schindelin H, Hänzelmann P, FEBS Lett. 589 (19PartA), 2578–2589 (2015). [PubMed: 26320413]

3. Meyer H, Weihl CC, J. Cell Sci 127, 3877–3883 (2014). [PubMed: 25146396]

4. Anderson DJ et al., Cancer Cell 28, 653–665 (2015). [PubMed: 26555175]

5. Banerjee S et al., Science 351, 871–875 (2016). [PubMed: 26822609]

6. Huyton T et al., J. Struct. Biol 144, 337–348 (2003). [PubMed: 14643202]

7. Davies JM, Brunger AT, Weis WI, Structure 16, 715–726 (2008). [PubMed: 18462676]

8. Bodnar NO et al., Nat. Struct. Mol. Biol 25, 616–622 (2018). [PubMed: 29967539]

9. Hänzelmann P, Schindelin H, Structure 24, 127–139 (2016). [PubMed: 26712278]

10. Tang WK, Odzorig T, Jin W, Xia D, Mol. Pharmacol 95,286–293 (2019). [PubMed: 30591537]

11. Han H, Hill CP, Biochem. Soc. Trans 47, 37–45 (2019). [PubMed: 30647138]

12. Schuberth C, Richly H, Rumpf S, Buchberger A, EMBO Rep. 5, 818–824 (2004). [PubMed: 15258615]

13. Han H et al., J. Biol. Chem 290, 13490–13499 (2015). [PubMed: 25833946]

14. Huang R, Ripstein ZA, Rubinstein JL, Kay LE, Proc. Natl. Acad. Sci. U.S.A 116, 158–167 (2019). [PubMed: 30584095]

15. Monroe N, Han H, Shen PS, Sundquist WI, Hill CP, eLife 6, e24487 (2017). [PubMed: 28379137]

16. Han H, Monroe N, Sundquist WI, Shen PS, Hill CP, eLife 6, e31324 (2017). [PubMed: 29165244]

17. Weith M et al., Mol. Cell 72, 766–777.e6 (2018). [PubMed: 30344098]

18. Hänzelmann P, Buchberger A, Schindelin H, Structure 19, 833–843 (2011). [PubMed: 21645854]

19. Han H et al., eLife 8, e44071 (2019). [PubMed: 31184588]

20. Bodnar NO, Rapoport TA, Cell 169, 722–735.e9 (2017). [PubMed: 28475898]

21. Blythe EE, Olson KC, Chau V, Deshaies RJ, Proc. Natl. Acad. Sci. U.S.A 114, E4380–E4388 (2017). [PubMed: 28512218]

22. Esaki M, Islam MT, Tani N, Ogura T, Sci. Rep 7, 5475 (2017). [PubMed: 28710470]

23. Puchades C et al., Science 358, eaao0464 (2017). [PubMed: 29097521]

24. de la Peña AH, Goodall EA, Gates SN, Lander GC,Martin A, Science 362, eaav0725 (2018). [PubMed: 30309908]

25. Dong Y et al., Nature 565, 49–55 (2019). [PubMed: 30479383]

26. Ripstein ZA, Huang R, Augustyniak R, Kay LE, Rubinstein JL, eLife 6, e25754 (2017). [PubMed: 28390173]

27. Gates SN et al., Science 357, 273–279 (2017). [PubMed: 28619716]

28. Deville C et al., Sci. Adv 3, e1701726 (2017). [PubMed: 28798962]

29. Yu H et al., Proc. Natl. Acad. Sci. U.S.A 115, E9560–E9569 (2018). [PubMed: 30257943]

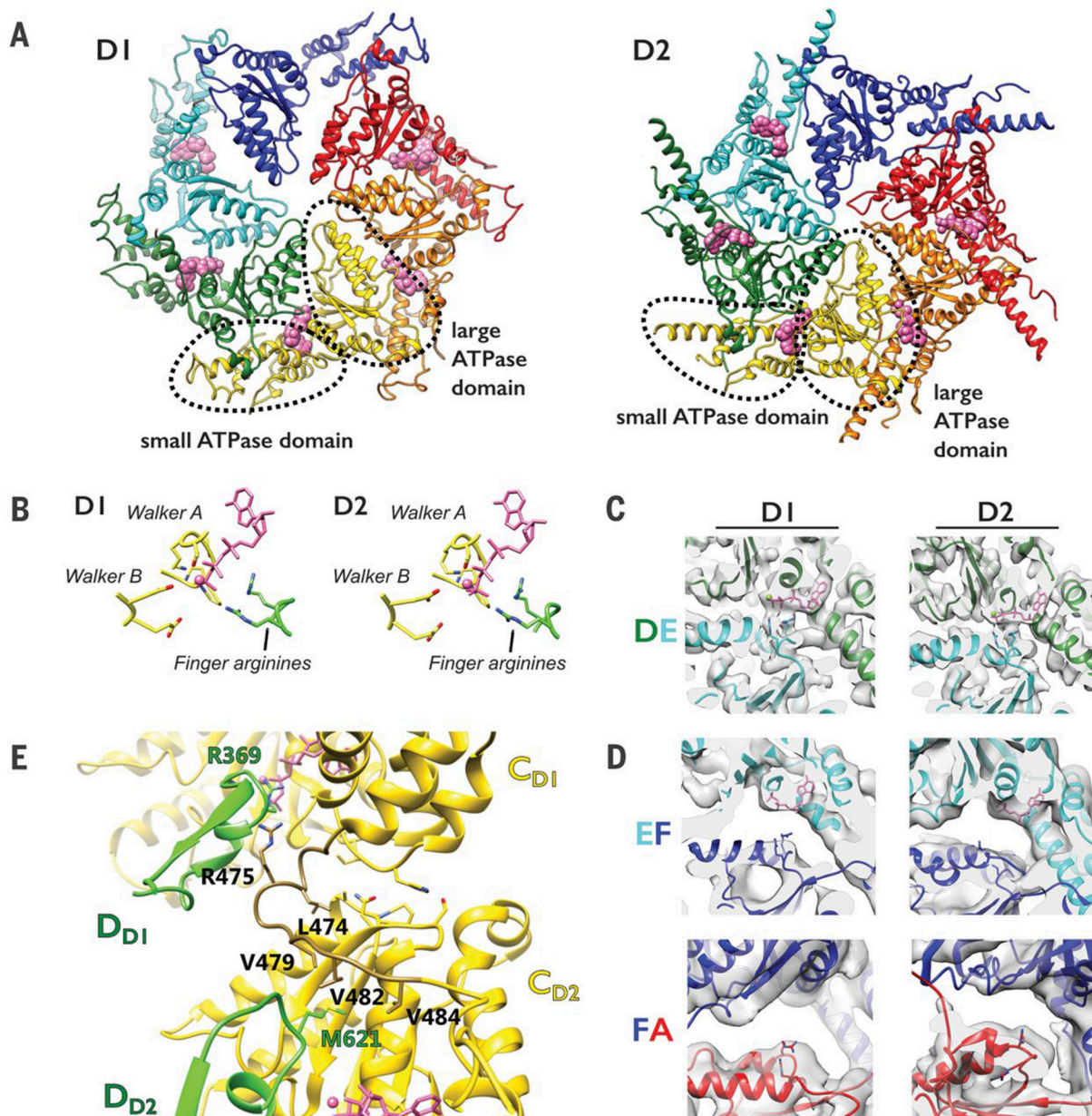30. White KI, Zhao M, Choi UB, Pfuetzner RA, Brunger AT, eLife 7, e38888 (2018). [PubMed: 30198481]

Fig. 1. Cryo-EM structure of the asymmetric Cdc48-Shp1-substrate complex.
(**A**) Cdc48 and Shp1 domain organization. Gray boxes indicate domains that are seen in the cryo-EM reconstruction. WA, Walker A; WB, Walker B; L1, pore loop 1, L2, pore loop 2; Arg, finger arginines. (**B** and **C**) High-threshold (B) and low-threshold (C) views of the cryo-EM reconstruction. Densities are segmented for the six Cdc48 subunit ATPase cassettes, N domains (tan), translocating substrate (magenta), and the Shp1 UBXdomain (orchid). Side-view densities are transparent in order to visualize substrate density in the pore. (**D**) Top and side views of the Cdc48-Shp1-substrate model in ribbon representation. Subunit C (yellow) is removed in the side view to visualize the substrate. (**E**) Model of Cdc48 (subunit B shown) with the associated Shp1 UBX domain, substrate, and nucleotides (pink spheres).
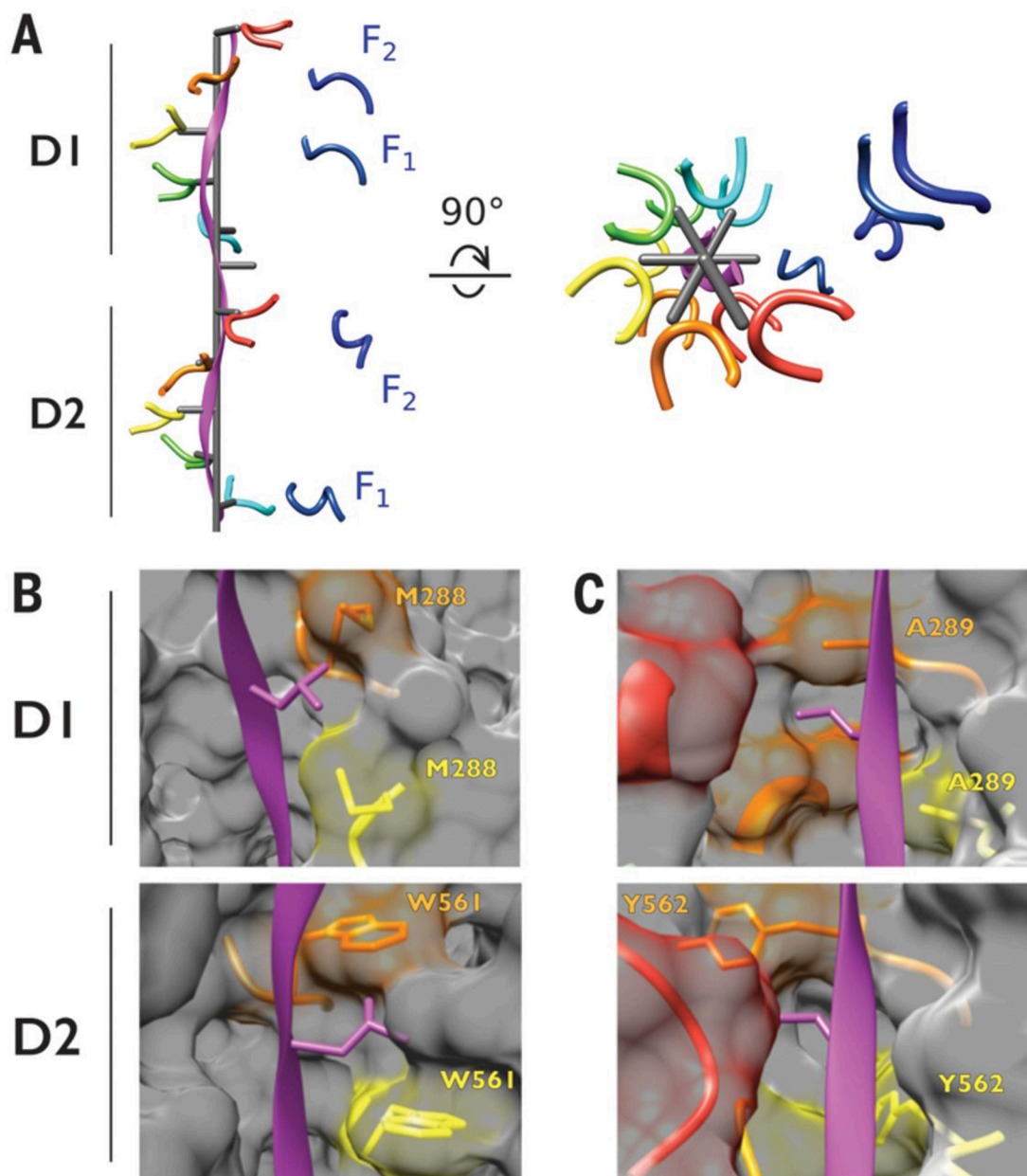
Fig. 2. Assembly of the D1 and D2 rings.
(**A**) D1 and D2 rings shown separately from the top with bound nucleotides (pink spheres).
(**B**) Nucleotide-binding pockets in D1 and D2. The CD interface is shown. The AB, BC, and
DE interfaces are very similar to each other (fig. S8). (**C**) Interfaces between large ATPase
domains of the helical subunits (A to E) are very similar to each other and are closely packed
(DE is shown). (**D**) The large domains of subunit F and its E and A neighbors do not pack
against each other (F$_1$ position is shown; F$_2$ is similar). (**E**) The linker between D1 and D2 is
very similar for subunits A to D (C is shown). Linker residues are in a darker shade of
yellow. D1 and D2 residues that mediate contacts between the rings are shown. Single-letter
abbreviations for the amino acid residues are as follows: A, Ala; L, Leu; M, Met; R, Arg; V,
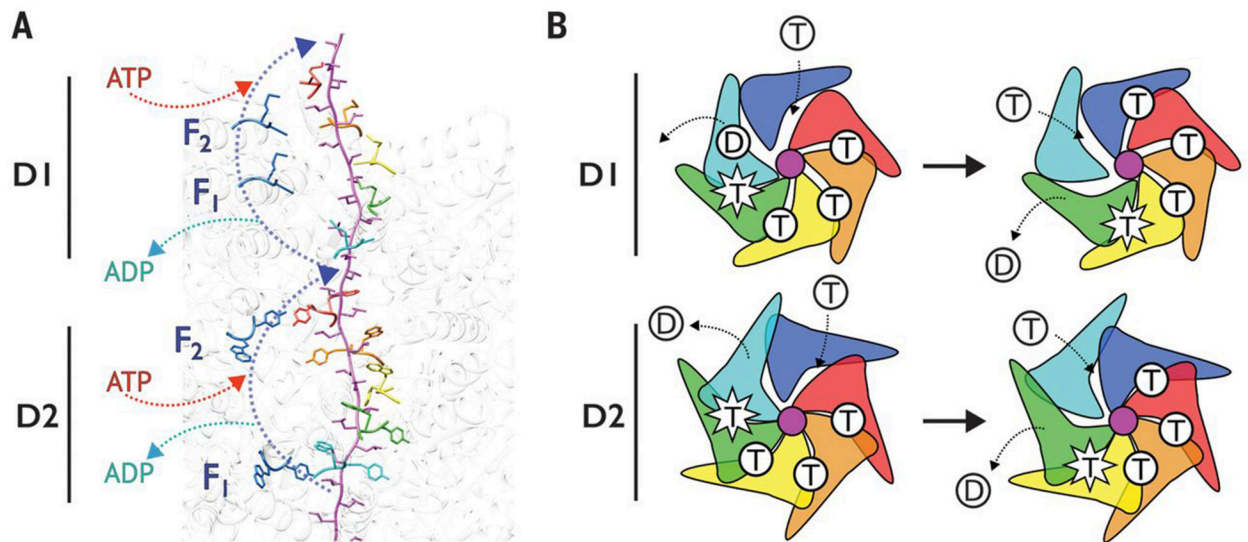Val; W, Trp; and Y, Tyr.

Fig. 3. Substrate interactions with the Cdc48 pore.

(A) Side and axial views of substrate and pore loop 1 residues. Subunit F is shown in both the F_1 and F_2 positions from focused classification. The helix axis is indicated with a gray rod. Helical spokes are positioned with 60° rotation and 6.8-Å translations. (B) Class 1 binding sites for the first residue of each substrate dipeptide and (C) class 2 binding sites for the second residue of each substrate dipeptide. The binding sites at the interface of subunits B and C are shown. The structure is very similar at the other (AB, CD, and DE) interfaces. For clarity, the substrate side chains are shown as leucine residues, although they are modeled as alanine or valine in the refined structure.
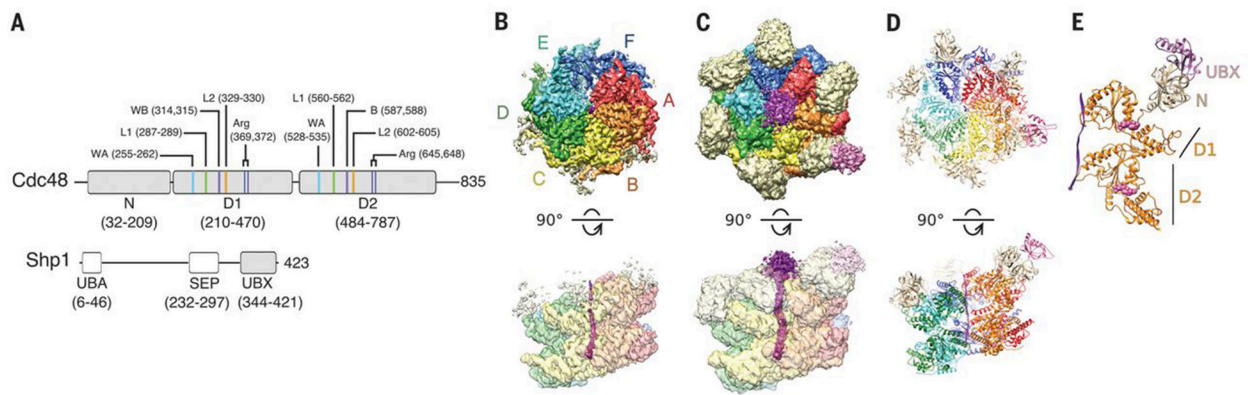
Fig. 4. Model of substrate translocation.

(A) Proposed trajectories of subunit F D1 and D2 domains from the substrate dipeptide following subunit E to the dipeptide preceding subunit A. (B) Model of nucleotide-induced substrate translocation. Each ATP hydrolysis reaction (starburst) advances the Cdc48 hexamer sequentially, such that each subunit assumes the state of its clockwise neighbor (from the top view). Nucleotide states: T, ATP; D, ADP.